All-optical carbon dioxide remote sensing using rare earth doped chalcogenide fibers

F. Starecki, A. Braud, J.-L. Doualan, J. Ari, Catherine Boussard-Plédel, Kristell Michel, Virginie Nazabal, P. Camy

All-optical carbon dioxide remote sensing using rare earth doped chalcogenide fibers

Florent Starecki[a], *Alain Braud*[a]*, *Jean-Louis Doualan*[a], *Julien Ari*[b], *Catherine Boussard-Plédel*[b], *Karine Michel*[c], *Virginie Nazabal*[b] *and Patrice Camy*[a]

[a] Laboratoire CIMAP UMR 6252 CEA-CNRS-Ensicaen, Université de Caen, 6 Boulevard du Maréchal Juin, 14050 Caen cedex 4, France

[b] Institut des Sciences Chimiques de Rennes, (ISCR), UMR-CNRS 6226, Université de Rennes 1, France

[c] BRGM, Bureau de Recherches Géologiques & Minières, 45060 Orléans, France

*Corresponding author: alain.braud@ensicaen.fr

Abstract

As many fundamental spectroscopic signatures associated to gases of interest are in the 2.5 – 15 µm spectral range (4000-350 cm^{-1}), gases can be detected using efficient infrared (IR) emissions from rare earth (RE) ions embedded into chalcogenide glasses, which are well-known for having low phonon energies. An all-optical IR fiber sensor for in-situ carbon dioxide monitoring was developed. The 4.3 µm mid-IR source probing the gas absorption in this sensor is a Dy^{3+} doped GaGeSbS fluorescent chalcogenide fiber. Following the 4.3µm partial absorption by CO_2, a wavelength conversion from 4.3 µm to 808 nm is implemented using excited state absorption (ESA) mechanisms in Er^{3+} doped GaGeSbS bulk glasses or fibers. This wavelength conversion allows the use of silica fibers to transport the 808 nm converted signal. This all-optical sensor with a sensitivity of few hundreds of ppm can be typically deployed over the kilometer range, making this tool suitable for field operations. The photon conversion principle used in this gas sensor could be implemented as a general mean to detect infrared radiations using visible or near-IR detectors instead of mid-infrared detectors.

Keywords

Chalcogenide fibers, wavelength conversion, rare earth, MWIR sources, CO_2 detection

1. Introduction

To decrease CO_2 atmospheric concentration to sustainable levels, carbon dioxide sequestration in field pilot sites is being investigated to assess the possibilities of large-scale underground storage [1]. Carbon Dioxide Capture and Storage (CCS) is recognized as a forthcoming technology for reducing CO_2 emissions requiring further research development to make CCS a sustainable and cost-effective technology. In this context, the European ECCSEL project is providing access for researchers to European research infrastructures devoted to second and third generation CCS technologies. Social acceptability of these industrial plants matters as they manage tons of carbon dioxide. The requirement for reliable CO_2 monitoring tools is thus essential for the CCS storage control, such as leaks sensors or pit CO_2 concentration probes.

For all these purposes, all-optical CO_2 detection system have key advantages over electronic devices, especially for high pressure working conditions and electromagnetic compatibilities, since there are no electronics parts within an all-optical CO_2 detection head. This concept features easiness of deployment and versatility, as this detection principle can be applied to the detection of numerous gases having mid-wave infrared (MWIR, 3-5 µm) or long-wave infrared (LWIR, 7-10 µm) absorption bands. Near infrared (NIR) optical carbon dioxide sensing devices for gas leak detection applications have already been demonstrated using DFB laser diodes [2].

Other optical compact infrared sensors with low power consumption have been developed for air quality monitoring and are based on blackbody IR sources and micro-bolometers for IR detection [3, 4]. Another technique for optical measurement of carbon dioxide in supercritical state is to use a fiber refractometer operating in the near-IR domain [5] which can be used as a remote sensing technique. None of these techniques can be considered as an all-optical detection system. To implement a true all-optical remote MWIR gas detection, an *in situ* wavelength conversion becomes necessary to convert the MWIR signal transmitted through the gas cell into a NIR signal. This NIR converted output signal can then be carried back to the measurement station with silica fibers presenting low optical losses.

Optical losses are indeed a key issue for remote detection using chalcogenide glasses fibers in the MWIR (3-5 µm). With a minimum value of about 50 dB/km [6], these fibers are clearly unsuitable for IR signal propagation over long distances. Our proposed alternative is to combine both advantages of the MWIR gas detection high sensitivity and the low-losses of silica fibers which enable a remote in-situ measurement of carbon dioxide concentration.

Rare-earth doped sulfide and selenide materials are suitable materials for the development of optical fiber sensors operating in the MWIR wavelength domain. These low-phonon energy materials allow both rare-earth (RE) doping and efficient MWIR luminescence and more importantly the fiber drawing of these rare-earth doped materials is well mastered [7, 8]. In a previous work, a Dy^{3+} doped GaGeSbS fiber was used as MWIR source to develop a CO_2 sensor prototype comprising electronic parts within

the sensor head such as an IR pyroelectric chip [9]. The work presented here consists in the development of an all-optical CO_2 sensor with the same type of MWIR fiber source while using another rare-earth doped chalcogenide fiber to convert into the NIR region the MWIR signal transmitted through the gas cell.

The broad emission bands of rare-earth doped glasses offers the possibility of differential detection techniques by carefully selecting two spectral windows within the emission band corresponding to the gas absorption and to a reference outside the gas absorption respectively. The principle of this all-optical sensor for MWIR carbon dioxide sensing is presented in Fig. 1 and comprises the Dy^{3+}: GaGeSbS MWIR source and a wavelength conversion device from 4.3 µm to 808 nm using an Er^{3+} doped GaGeSbS fiber [10].

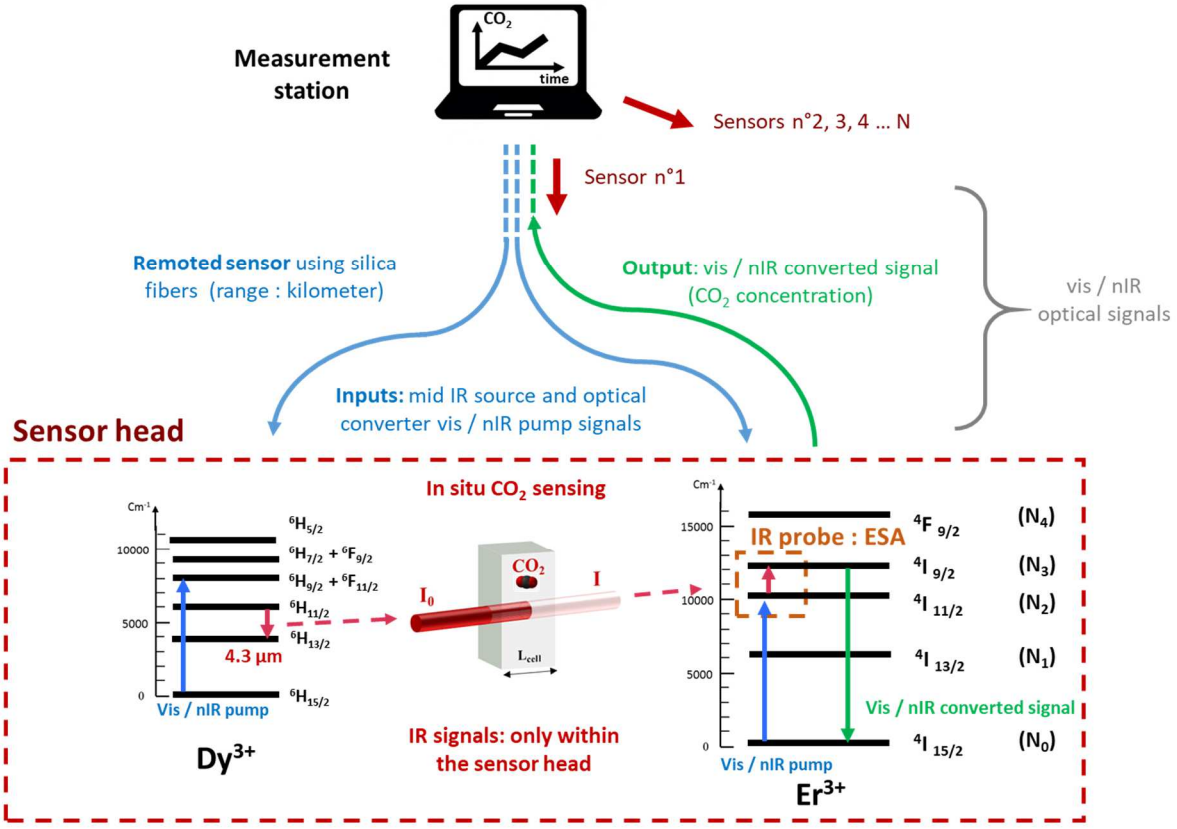

Fig. 1: overview of the MWIR CO_2 remote sensor based on rare earth luminescence as MWIR source (Dy^{3+}) and as MWIR to visible wavelength converter (Er^{3+}).

This sensor operates as follows: starting from the measurement station, a NIR laser diode beam is sent via a silica fiber (blue line in Fig. 1) to optically pump the Dy^{3+} doped GaGeSbS fiber located within the sensor head. This in-situ fiber generates the MWIR probe beam, which passes through the gas cell and then is injected in the wavelength conversion device, consisting in an Er^{3+} doped GaGeSbS fiber pumped by a second fibered NIR laser diode (blue line in Fig. 1). Following this pumping, Er^{3+} ions are excited into the $^4I_{11/2}$ level; the incoming MWIR photons are then absorbed by the Er^{3+} $^4I_{11/2} \rightarrow {}^4I_{9/2}$

excited state absorption transition. Er^{3+} ions now in the $^4I_{11/2}$ manifold, a subsequent spontaneous emission takes place mainly around 808 nm as it is the dominant radiative transition from the $^4I_{11/2}$ level [10]. The 808 nm intensity being proportional to the MWIR signal intensity, this mechanism represents an effective MWIR to visible photon conversion process.

The converted signal at 808 nm is collected by a silica fiber and carried back to the measurement station (green line in Fig. 1), forming an "all-optical" detection system since the detection head only includes optical elements. As only a single set of electronic devices comprising two laser diodes and a photomultiplier tube is necessary to operate several sensing heads, a single measurement station could perform the carbon concentration mapping of a wide area such as a geological CO_2 storage site.

2. Materials and methods

2.1. Glass fabrication, fiber drawing and crystal growth

The chalcogenide glass synthesis process is based on conventional melting / quenching methods [7]. Raw materials of high purity (5N, 3N rare-earth sulfides) were placed in silica ampoules and pumped under vacuum for hours. After sealing and homogenization at 850°C using a rocking furnace, the glass rods were water quenched and annealed at a temperature close to $T°_g$. Glass transition and crystallization temperatures ($T°_g$ and $T°_x$) were determined using differential scanning calorimetry. Following that process, 1000 ppm Dy^{3+} doped GaGeSbS and 15000, 5000 and 2000 ppm Er^{3+} doped GaGeSbS glasses were elaborated. Single core glass fibers were drawn from the 1000 ppm Dy^{3+} doped GaGeSbS and 2000 ppm Er^{3+} doped GaGeSbS preforms. The sensor prototype is based on fibered materials. For field operations, coated fibers were used with a 60 µm thick UV-cured polymer coating deposited on the fibers, enhancing the fibers mechanical properties [11]. Both fiber ends were mounted in FC/PC connectors and polished.

2.2. Sensor development

The all-optical carbon dioxide sensor comprising either a bulk or fibered based wavelength conversion device is presented in Fig. 2. The MWIR probe signal at 4.3µm results from the guided emission of a 1000 ppm Dy^{3+}: GaGeSbS fiber. This 130 mm long and 350 µm diameter fiber is pumped by a Q-Photonics 1320 nm laser diode. In order to measure the fiber 4.3µm output power, a Gentec XLP12 power meter was used along with several bandpass or long pass filters to isolate the power meter from background intensities due to thermal loads on the optical filters.

Due to the high material refractive index of the single core chalcogenide fiber (n=2.3), the output IR beam is emitted through 2π srd [12]. A key issue for the detector efficiency is of course to maximize the infrared power transmitted through the gas cell and then injected in the conversion fiber. Therefore, a short focal commercial aspheric lens with a 0.85 numerical aperture was used to ensure the collection

of the Dy^{3+} fiber output IR signal. This IR output beam is then collimated using a high numerical aperture (NA) aspheric lens with 3-5 µm AR coatings (Thorlabs C037TME-E). Within the broad MWIR $^6H_{11/2} \rightarrow {}^6H_{13/2}$ Dy^{3+} emission band, the CO_2 absorptive part is isolated using a 4.3 µm centered band-pass filter (FWHM of 200 nm). The IR signal then passes through the gas cell equipped with CaF_2 windows, and is partially absorbed by the carbon dioxide before being injected in the Er^{3+} doped conversion material using a short focal distance AR-coated lens (Lightpath 390093-IR3). This Er^{3+} doped bulk glass or optical fiber is simultaneously pumped at 980 nm to excite Er^{3+} ions in the $^4I_{11/2}$ manifold using a laser diode (Axcel Photonics) with a typical incident power of few hundred milliwatts.

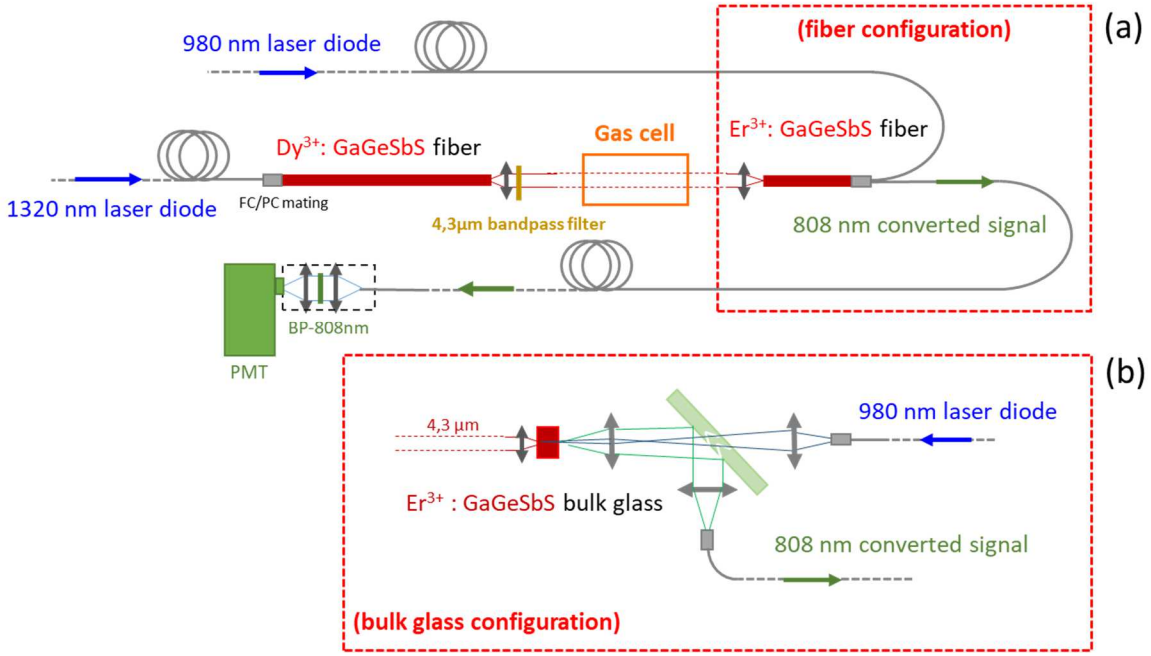

Fig. 2: Sensor scheme (a): fiber configuration; (b): bulk glass configuration

As explained earlier (Fig. 1), an excited state absorption (ESA) of the transmitted 4.3 µm signal takes place in the conversion material, from the $^4I_{11/2}$ to the $^4I_{9/2}$ excited states. The subsequent emission at 808 nm from the $^4I_{9/2}$ excited state is proportional to the 4.3 µm signal. Therefore, the conversion procedure consists in measuring this 808 nm emission intensity. Conversion experiments were conducted using 15000 and 5000 ppm Er^{3+} doped GaGeSbS bulk glasses, which could not be drawn as fibers, and 2000 ppm Er^{3+} doped fibers. Optical fiber and bulk glass experimental setups for the wavelength conversion are presented in Fig. 2(a) and Fig. 2(b) respectively. The incident MWIR beam is injected through one face, while the 980 nm Er^{3+} pump and the 808 nm converted signal are respectively injected and collected through the material other end face with the use of a silica fiber bundle (Fig. 2(a)) or a dichroic mirror (Fig. 2(b)). In Fig. 2(b), the bulk glass based conversion device comprises a 900 nm long-pass dichroic mirror, separating the Er^{3+} pump laser from the 808 nm converted signal. A short focal length half ball sapphire lens is used for both the injection of the pump and the collimation of the converted signal, which is then coupled into a 600 µm diameter core silica fiber using visible AR coated lenses.

After what, the 808 nm converted signal is further isolated using a narrow bandpass filter (Spectrogon BP-808-026nm), and then detected using a Hamamatsu R3896 photomultiplier tube. Output electric signals are then passed through a low noise amplifier (Femto DLPCA-200) and a lock-in amplifier (Stanford Research SR830) connected to a computer via its GPIB link. A dedicated LabVIEW software was developed to monitor the sensor key parameters. All fibers are mounted in FC/PC connectors with both end faces polished. In order to build a field operation prototype, the fiber robustness had to be enhanced, and all the optical fibers were mounted in 3 mm standard tubing. The detector housing outer diameter is 125 mm, and is periodically drilled to enable a homogeneous gas circulation within the housing. For field operations, the designed prototype is equipped with a reference arm for long-term measurement stability, which could be affected by temperature variations. During field sensing experiments in CO_2 storage pits, temperature variations can be up to 20° from the surface to the bottom of the pit, which impacts the sensor efficiency.

The reference arm is the duplication of the measurement arm, with additional Dy^{3+} MWIR fiber source and Er^{3+} converting fiber. A 4.5 µm long-pass filter is used to isolate within the Dy^{3+} emission band a spectral window free of carbon dioxide absorption, so that the converted intensity from the reference arm does not depend on the carbon dioxide concentration. This reference arm requires its own PMT, preamplifier, and lock-in amplifier. The subsequent differential measurement consists in recording the relative intensity variation of the reference arm, and then dividing the measurement arm intensity value by the reference arm intensity value in real time. For these two channels, the converted signal is denoted Ic, and represents the 808 nm signal variations recorded at the probe frequency.

For the gas detection experiments performed in the laboratory prior to the field experiments, a sealed housing was used with specific inlet and outlet for gas circulation. The prototype was calibrated using successive injections of carbon dioxide mixes and nitrogen flushes. The free space optical paths are 18 and 13 cm for the measurement and reference arms respectively. Corresponding converted signal variations and signal to noise ratio were recorded in real time with a time constant of few seconds. The prototype was calibrated over a wide range of carbon dioxide concentrations. 2000 ppm, 2%, 10% and 100% carbon dioxide cylinders were used, and a nitrogen / CO_2 gas mixer was implemented to regulate carbon dioxide concentrations from 10 to 100%. CO_2 concentrations ranging between 1% and 100% were simultaneously measured at the gas cell exit using a Geotech G100 commercial device.

3. Results

3.1. Sensor calibration

The previous results led to the development of a carbon dioxide prototype for field experiments comprising a Dy^{3+}: GaGeSbS MWIR emitting fiber and an Er^{3+}: GaGeSbS conversion fiber. Carbon dioxide sensing experiments were performed using this all-optical sensor for various CO_2 concentrations

ranging from 2000 ppm to 100% CO_2. The sensitivity over this range can be estimated using the signal to noise ratio analysis in steady-state regime. The 2σ sensitivity S is given as $S=2.X_{CO2}/R$, where X_{CO2} is the CO_2 concentration injected in the cell. Fig. 3(a) shows the converted intensity Ic variations following different gas injections, each of them being followed by a nitrogen purge of the 18 cm gas cell placed between the MWIR source and the converter. Fig. 3(b) reports the corresponding calculated sensitivities as a function of the CO_2 concentration.

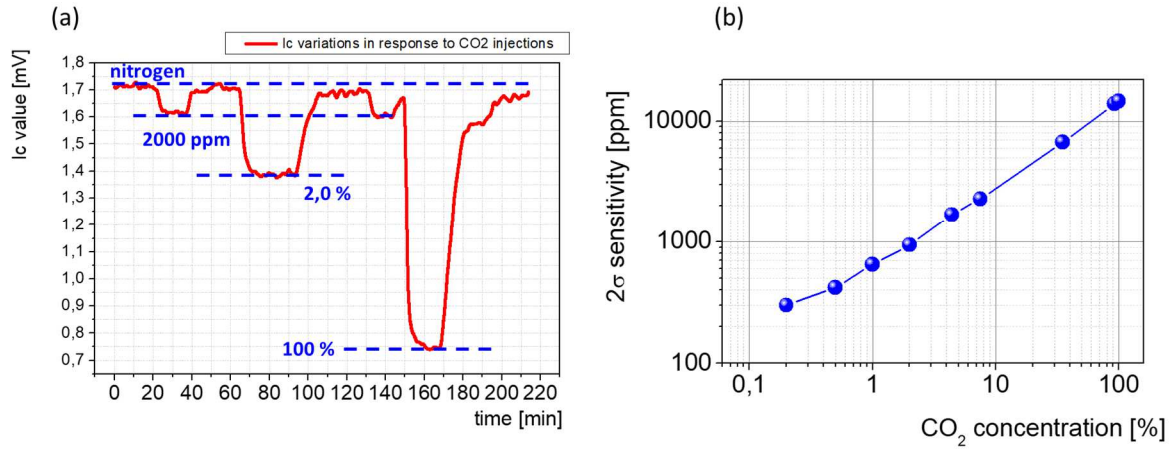

Fig. 3: prototype carbon dioxide calibration: (a) converted signal output variations following carbon dioxide injections. (b) calculated sensitivity as a function of the CO_2 concentration.

The prototype carbon dioxide sensitivities are about 300 ppm over the 0-2000 ppm CO_2 range, 1000 ppm for 1% CO_2 and 3000 ppm for 10% CO_2. The relative accuracy, expressed as S/X_{CO2}, is less than 15% for low CO_2 concentrations (< 2000 ppm) and going from 3% to 1% in the 2% - 100% CO_2 range.

3.2. Prototype field operation

The sensor prototype was tested in a 100-m depth dry pit at the LSBB facility (Laboratoire Souterrain à Bas Bruit) in Rustrel, France. A crane was used to move the detector up and down the pit. The connection cable is composed of four 100-m long silica fibers. Gas pipes were attached to the detector body and a surface Geotech G100 commercial device was used to assess the CO_2 concentration at the detector location. The whole device is presented in Fig. 4(a), while Fig. 4(b) reports a CO_2 concentration measurement as a function of the depth in the pit.

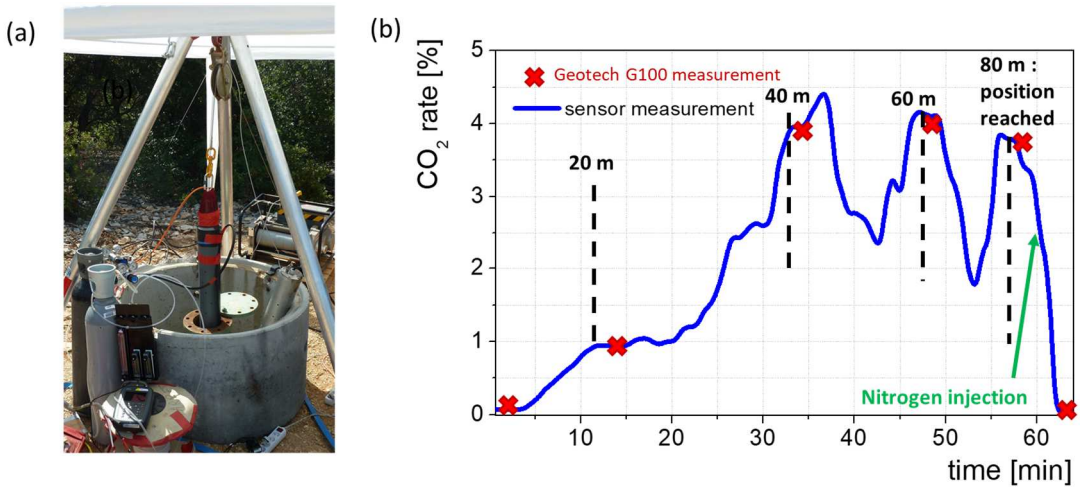

Fig. 4: (a): prototype (grey tube) being inserted in the pit; (b): CO_2 measurement performed with the all-optical sensor. Red crosses are the Geotech measurements points.

The sensor was translated through a CO_2 gas plume that was previously injected during a separate field testing session. This all-optical prototype operates in-situ in real-time while the Geotech G100 sensor is located outside the pit and requires to pump out the gas from the pit. Therefore, the Geotech 100 measurements are delayed by few minutes in comparison with our all-optical sensor. Steady state regime measurements comparisons were performed. The sensor was stopped at several depths: 20, 40, 60 and 80 m which was the final depth. At this depth, a nitrogen injection was performed locally, and the corresponding CO_2 concentration measurements went both back to zero (Fig. 4(b)). During the whole process, the two CO_2 content measurements remained in good agreement, which further supports the potential of this all-optical detector to be deployed as a CO_2 field sensor with uncommon features at a reasonable cost.

4. Discussions

4.1. MWIR source at 4.3µm

Throughout the experiments presented in this work the same 1000 ppm Dy^{3+} doped GaGeSbS MWIR fiber source was used. The 130 mm fiber length leads to the absorption of almost the entire 1320 nm pumping signal. After collimation, the 4.3 µm ($^6H_{11/2} \rightarrow {}^6H_{13/2}$ transition) Dy^{3+} doped chalcogenide fiber output power is 80 µW. The efficiency of this IR emission strongly depends on the glass matrix and its maximal phonon energy. Here, sulfide glasses because of their low phonon energy are known to be suitable for MWIR luminescence generation [13]. In a previous report, a Dy^{3+} doped fiber was pumped by a 915 nm laser diode ($^6H_{15/2} \rightarrow {}^6H_{7/2}$ transition) [9, 12], while in this work a 1320 nm laser diode ($^6H_{15/2} \rightarrow {}^6H_{9/2}$ transition) is used. The $^6H_{11/2}$ level excitation using either a 1320 or 920 nm pumping is achieved with a comparable efficiency since in both cases it is mainly due to non-radiative relaxations from the $^6H_{9/2}$ manifold to the $^6H_{11/2}$ level. The Dy^{3+} absorption cross section is about 3.5 times higher

at 1320 nm than at 915 nm. The advantage of having a higher absorption cross section is to enable the use of shorter rare-earth doped chalcogenide fibers. The typical fiber attenuation at 4.3 µm is few dB/m because of impurities like S-H absorption tails [7].Therefore by reducing the fiber length, one can increase the output infrared power by decreasing the attenuation losses.

The Dy^{3+}: GaGeSbS fiber emission spans from 4 to 4.6 µm, and is affected by CO_2 absorption lines from 4.19 to 4.45 µm, so that a differential detection technique can be implemented using the same emission band. To do so, the integrated fluorescence intensity above 4.45 µm is used as a reference within the sensor reference arm discussed earlier. The dashed line in Fig. 5(a) illustrates the separation between domains (1) and (2), standing for the measurement and reference spectral domains respectively.

Thus, this all-fibered solution using standard FC/PC mating sleeves provides robustness and drastically reduces the necessity of optical alignments, making it far more suitable for field operations than bulk glasses based devices.

4.2. Er^{3+} MWIR to NIR wavelength conversion

Depending on the carbon dioxide concentration, the MWIR signal is partially absorbed within the gas cell, and the remaining signal is then injected in the conversion material. As explained earlier (Fig. 1), the wavelength conversion from 4.3 µm to 808 nm is based on the Er^{3+} excited state absorption (ESA) of the Dy^{3+} infrared emission. Therefore, this conversion mechanism depends on the overlap between the Dy^{3+}: GaGeSbS emission band and the Er^{3+}: GaGeSbS excited state absorption spectrum, which is shown in Fig. 5(a).

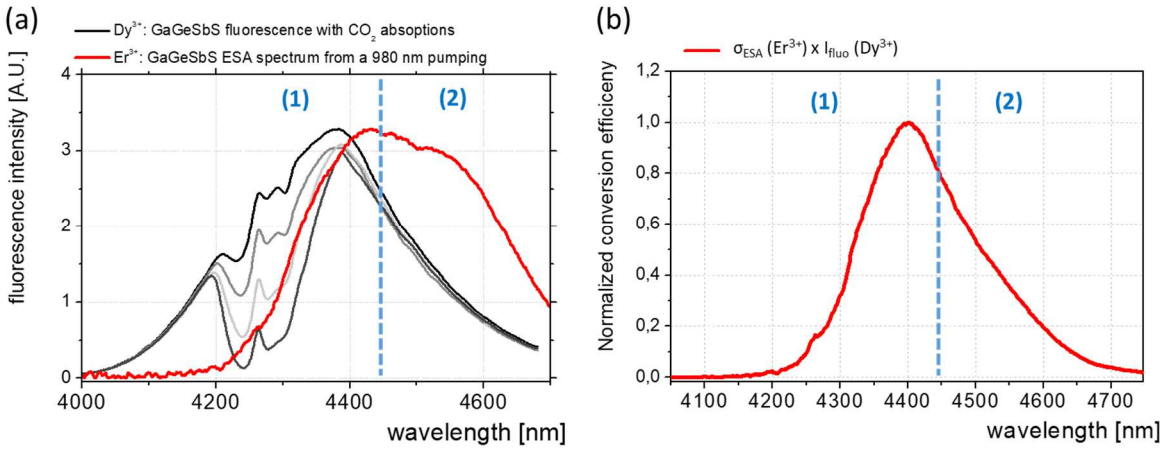

Fig. 5: (a): Dy^{3+}: GaGeSbS (with CO_2 absorption dips for different CO2 concentrations) emission band and Er^{3+} : GaGeSbS excited state absorption spectrum. (b): spectral overlap between the Er^{3+} ESA and Dy^{3+} luminescence, indicating the wavelength conversion relative efficiency over this spectral domain.

The spectral overlap between the Dy^{3+} emission and the Er^{3+} ESA cross-section spectra represents the conversion relative efficiency and is expressed as $I_{fluo}(Dy)$ x $\sigma_{ESA}(Er)$ as depicted in Fig. 5(b). The wavelength conversion reaches its maximum efficiency at 4.4 µm and the dashed line shows that the

conversion can be performed efficiently in the two defined spectral domains (1) and (2) with and without carbon dioxide absorption respectively. This spectrum thus validates the use of a differential measurement technique with these two spectral domains.

The conversion efficiency is temperature-dependent, since RE spectroscopic properties such as the multiphonon relaxation rate depend on temperature. The reference arm (domain (2)) main function is to correct the measurement signal from temperature variations. The measurement and reference arms discussed earlier give access to conversion signals from domains (1) and (2) from two distinct Er^{3+} doped conversion fibers. At the output of these conversion fibers, the 808 nm converted signal is emitted through 2π srd and the collected fraction of 808 nm converted signal is limited to photons entering the collection fiber within the fiber bundle (Fig. 2(a)).

This ESA based conversion process requires low phonon energy materials to provide long RE energy level lifetimes and a high MWIR luminescence quantum efficiency. Additionally, the host must be transparent at the converted signal wavelength and the rare earth excited state absorption cross section must be high enough to ensure an efficient photon addition. Er^{3+} ions embedded in the $Ga_5Ge_{20}Sb_{10}S_{65}$ chalcogenide glass matrix match all these criteria. With a 64% quantum efficiency for the $^4I_{9/2}$ emitting level combined with a 0.8 branching ratio for the Er^{3+} $^4I_{9/2} \rightarrow {}^4I_{15/2}$ transition at 808 nm, an efficient converted emission following the ESA process is ensured [7].

An analytical description of the conversion process was published by our group in Er^{3+} doped chalcogenide glasses [10]. A theoretical analysis of the wavelength conversion process involves the use of a set of rate equations and signal propagation equations for the converting fiber. The two main energy levels at the core of this conversion mechanism are the $^4I_{9/2}$ and $^4I_{11/2}$ levels (Fig.1). Thus, the rate equations for the $^4I_{9/2}$ and $^4I_{11/2}$ levels in steady-state regime are given in Eq. 1 and Eq. 2 respectively, For the sake of clarity the energy transfers taking place among Er^{3+} ions are not shown here.

$$N_4 \cdot (A_{43}^R + A_4^{MP}) + A_{53}^R \cdot N_5 - \frac{N_3}{\tau_3} + \sigma_{ESA} \cdot \Phi_{IR} \cdot N_2 = 0 \qquad \text{(Eq. 1.)}$$

$$N_3 \cdot (A_{32}^R + A_3^{MP}) + A_{42}^R \cdot N_4 + A_{52}^R \cdot N_5 - \frac{N_2}{\tau_2} + \sigma_p \cdot \Phi_p \cdot N_0 - \sigma_{ESA} \cdot \Phi_{IR} \cdot N_2 = 0 \qquad \text{(Eq. 2.)}$$

$N_{0,2,3,4,5}$ stands for the $^4I_{15/2}$, $^4I_{13/2}$, $^4I_{11/2}$, $^4F_{9/2}$, and $^4S_{3/2}$ level populations. τ_3 and τ_2 are the $^4I_{9/2}$ and $^4I_{11/2}$ level lifetimes respectively. A^R_{ij} are the radiative decay rates from i to j manifold, while A^{MP}_i are the multiphonon relaxation rates of the i manifold. $\sigma_{p,}$ and σ_{ESA} are the $^4I_{15/2} \rightarrow {}^4I_{11/2}$ and $^4I_{11/2} \rightarrow {}^4I_{9/2}$ absorption and excited state absorption cross sections respectively. $\Phi_{p,IR}$ represents the pump and infrared probe photon fluxes in $cm^{-2}.s^{-1}$.

The propagation equation along the fiber (z-axis) for the 808 nm converted signal power (P_{30}) generated by the $^4I_{9/2} \rightarrow {}^4I_{15/2}$ spontaneous emission is as follows.

$$\frac{dP_{30}}{dz} = \left(\sigma_{30} \cdot N_3 - \sigma_{03} \cdot N_0 - \alpha_{p30}\right) \cdot P_{30} + A_{30}^R \cdot \eta \cdot h \cdot \nu_{30} \cdot S_f \cdot N_3 \qquad \text{(Eq. 3.)}$$

where the last term $A_{30}^{R} \cdot \eta \cdot h \cdot \nu_{30} \cdot S_f \cdot N_3$ represents the fraction of emitted light at 808nm which is guided throughout the fiber. $h\nu_{30}$ is the photon energy at 808 nm, S_f the fiber surface and η the guiding solid angle for the spontaneous emission. The fluorescence at 808 nm is first emitted through the whole solid angle, but only a η light fraction satisfies the guiding conditions defined by total internal reflection within the fiberand thus reaches the fiber end face. α_{p30} represents the fiber background propagation losses at 808 nm which is a limiting factor for the fiber length, Because of the exponential decrease in the pump absorption along the fiber, the end of a long fiber cannot be excited and does not emit light. However, the guided light coming from the pumped part of the fiber is affected by the propagation losses in this non-pumped zone. Thus, in our experiments we have deliberately used short converting fibers typically around 80 mm to minimize this effect.

Besides the desired wavelength conversion process, parasitic signals also take place at the converting wavelength (808 nm) without any MWIR signal entering the converter. The converter material is excited at 980 nm and the Er^{3+} particular energy levels distribution allows the excitation of Er^{3+} ions to the higher lying $^4F_{7/2}$ manifold through upconversion processes [14] followed by their non-radiative relaxation to the $^4S_{3/2}$ manifold. From this $^4S_{3/2}$ level non-radiative and radiative processes lead to the population of the $^4I_{9/2}$ level which emits at 808 nm. Therefore, the pump itself at 980 nm gives rise to a parasitic 808 nm emission [10] at the pump modulation frequency. This pump related 808 nm emission is much brighter than the 808 nm converted signal coming from the 4.3 µm ESA, but both contributions can be discriminated from one another using two distinct modulation frequencies for the pump at 980 nm and the probe at 4.3µm. In order to assess the impact on the converted signal to noise ratio (SNR) of this parasitic pump-related emission, we recorded simultaneously the converted and pump-related intensities, labelled Ic and Ip respectively, by using two lock-in amplifiers, one at each modulation frequency. The noise is taken as the converted signal noise standard deviation (SD) in steady state regime and the SNR is defined as SNR = $V_{probe\ ON}$ / SD where $V_{probe\ ON}$ is the lock-in amplifier output voltage at the MWIR probe modulation frequency. Using a fixed IR probe input, the converted signal to noise ratio was recorded for different pumping powers at 980nm. At the same time, the Ip and Ic values were recorded, so as to simultaneously measure the Ic/Ip ratio. These data enable to plot the conversion signal to noise ratio as a function of the Ic/Ip ratio (Fig. 6). The SNR is proportional to the sensor sensitivity, and Fig. 6 shows its trend with respect to the Ic / Ip ratio.

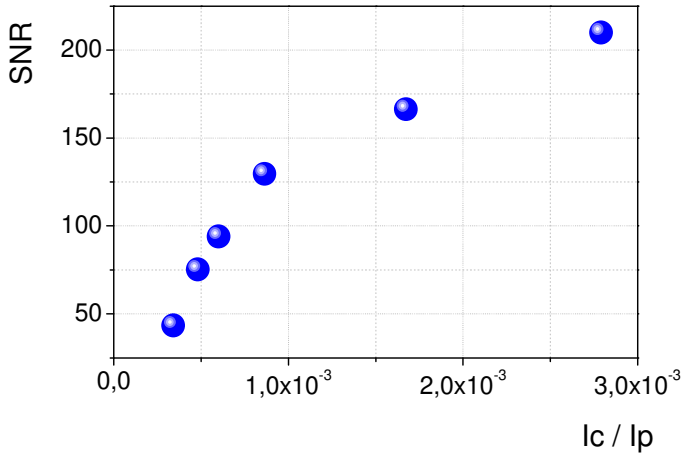

Fig. 6. Converted signal to noise ratio measured in a fiber configuration sensor (2000 ppm doped Er^{3+} doped GaGeSbS fiber) as a function of I_c/I_p.

For a given IR probe input, a converter optimum pumping power exists. Basically, a high pumping power leads to a higher Er^{3+} $^4I_{11/2}$ population, and thus to a higher converted intensity through the $^4I_{11/2} \rightarrow {}^4I_{9/2}$ ESA. But, as demonstrated in ref. 7, Ip exhibits a square dependence with the pumping power, while Ic has a linear dependence as shown in Eq.2 by the linearity between the pump power flux and the $^4I_{9/2}$ emitting level population. As a consequence, the Ic/Ip ratio increases when the pumping power decreases. Fig. 6 shows that the maximum SNR is achieved for higher value of Ic/Ip meaning for low pumping powers. This non-intuitive result illustrates the relevance of Fig. 6. However, by drastically reducing the pumping power, I_p and I_c reach very low values. In that case the SNR starts to deteriorate since intrinsic electronic noises ultimately dominate the signal measurement. In our case, a good compromise is found by using a pumping power at 980 nm of few hundreds milliwatts.

Besides the optimization of the pumping power, the length and doping level of the converting fiber are important parameters to optimize. We intentionally limited the Er^{3+} concentration at 2000 ppm within the fiber in order to limit the impact of upconversion processes and energy transfers on the converted signal. This low doping level imposes the use a long enough fiber to ensure an efficient pumping of the fiber. However, sulfide fiber background losses are typically of 20 dB/m around 800nm [7]. As discussed earlier, for a better conversion efficiency, short fiber are preferable, which minimizes the fiber losses effect on the converted fluorescence signal. Optimal conditions for an efficient conversion process were found in our experiments by using 8 mm long fibers and keeping a 2000 ppm doping level.

4.3. Carbon dioxide sensor elaboration and calibration

Building on the previous wavelength conversion results, all-optical carbon dioxide sensing experiments were performed with various conversion setups (Fig. 2). A 10-cm long gas cell was placed on the optical path between the MWIR source and the converter. To assess the potential of different sensor configurations, nitrogen gas followed by 100% carbon dioxide were injected in the cell. From this single

0 to 100% CO_2 concentration response test, a ratio R was calculated which is defined as the signal variation from the purged cell to the 100% CO_2 containing cell (V_{N2} - V_{CO2}) divided by the standard deviation (SD) of the converted signal intensity in steady state regime ($R=(V_{N2}-V_{CO2})/SD$). This R value reflects the signal to noise ratio and thus the detector sensitivity. This experiment was performed with Er^{3+} doped fibers and Er^{3+} doped bulk glasses, enabling the use of highly doped materials which cannot be drawn as fibers. Frequency conversion results with the use of either bulk or fibered Er^{3+}: $Ga_5Ge_{20}Sb_{10}S_{65}$ glasses are reported in the Table 1.

Er^{3+} $Ga_5Ge_{20}Sb_{10}S_{65}$	dopant [ppm]	thickness [mm]	R
bulk glass	15000	1,5	92
bulk glass	5000	1,5	97
fiber	1000	120 (length)	309

Table 1. Conversion signal to noise ratios obtained for bulk and fiber based wavelength conversion setups.

Table 1 shows that even with bulk glasses, the all-optical detection of CO_2 was successful. However, the R value indicates that the signal to noise ratio is better when using an Er^{3+} doped fiber. As expected, the spatial overlap between the incoming 4.3 µm radiation and the pump beam is much better within a fiber than in a bulk material. Moreover, because of the high chalcogenide refractive index the converted emission at 808 nm is efficiently guided, resulting in a higher signal to noise ratio than in bulk samples (Table 1). Nonetheless, the successful use of bulk glass based conversion devices show that they could be implemented in a future gas sensor if the necessary converting material cannot be drawn as a fiber. For the prototype development, depending on the targeted application, the gas cell length could be modified to further tune the sensitivity curve. Our single pass gas cell has a relatively short optical path compared to other multi-pass optical detectors. Sensitivity could be enhanced for instance through the use of resonators (ICOS) as reported in the literature [15].

Conclusions

In conclusion, we have demonstrated here the operation of an all-optical in-situ carbon dioxide field sensor based on rare earth doped chalcogenide fibers used as MWIR source and frequency conversion device. The spontaneous guided emission of a Dy^{3+}: GaGeSbS fiber was used to probe CO_2 at 4.3 µm followed by the wavelength conversion of the 4.3 µm transmitted signal into an 808 nm signal using excited state absorption properties in Er^{3+}: GaGeSbS.

This detector offers a real-time remote sensing capability up to the kilometer range with the use of standard silica fibers, making it a convenient tool for continuous monitoring of carbon dioxide over wide areas with a minimum sensitivity of 300 ppm. Field operation proved the pertinence of using this MWIR remote detector for in-depth CO_2 storage applications. The conversion principle implemented in this

sensor was also demonstrated with highly doped bulk Er^{3+}: GaGeSbS glasses, allowing the development of various optical designs for the wavelength conversion device. These promising results supports further investigations on the development of conversion based all-optical sensors operating at different wavelengths in the mid or long wave IR domain.

Acknowledgments

The authors acknowledge the collaboration with IDIL Fibres Optiques and BRGM and the funding through the ADEME COPTIK project.

References

[1] J. Alcalde, I. Marzán, E. Saura, D. Martí, P. Ayarza, C. Juhlin, et al., 3D geological characterization of the Hontomín CO2 storage site, Spain: Multidisciplinary approach from seismic, well-log and regional data, Tectonophysics, 627(2014) 6-25.

[2] D. Fan, J. Gong, B. Dong, A. Wang, Remote CO2 leakage detection system, Optical Engineering, 52(2013) 010502-.

[3] J. Hodgkinson, R. Smith, W.O. Ho, J.R. Saffell, R.P. Tatam, Non-dispersive infra-red (NDIR) measurement of carbon dioxide at 4.2 μm in a compact and optically efficient sensor, Sensors and Actuators B: Chemical, 186(2013) 580-8.

[4] P. Barritault, M. Brun, O. Lartigue, J. Willemin, J.-L. Ouvrier-Buffet, S. Pocas, et al., Low power CO2 NDIR sensing using a micro-bolometer detector and a micro-hotplate IR-source, Sensors and Actuators B: Chemical, 182(2013) 565-70.

[5] G. Burton, L. Melo, S. Warwick, M. Jun, B. Bao, D. Sinton, et al., Fiber refractometer to detect and distinguish carbon dioxide and methane leakage in the deep ocean, International Journal of Greenhouse Gas Control, 31(2014) 41-7.

[6] Z. Tang, V.S. Shiryaev, D. Furniss, L. Sojka, S. Sujecki, T.M. Benson, et al., Low loss Ge-As-Se chalcogenide glass fiber, fabricated using extruded preform, for mid-infrared photonics, Opt Mater Express, 5(2015) 1722-37.

[7] V. Moizan, V. Nazabal, J. Troles, P. Houizot, J.-L. Adam, J.-L. Doualan, et al., Er3+-doped GeGaSbS glasses for mid-IR fibre laser application: Synthesis and rare earth spectroscopy, Optical Materials, 31(2008) 39-46.

[8] S. Cui, C. Boussard-Plédel, J. Lucas, B. Bureau, Te-based glass fiber for far-infrared biochemical sensing up to 16 μm, Opt Express, 22(2014) 21253-62.

[9] F. Starecki, F. Charpentier, J.-L. Doualan, L. Quetel, K. Michel, R. Chahal, et al., Mid-IR optical sensor for CO2 detection based on fluorescence absorbance of Dy3+:Ga5Ge20Sb10S65 fibers, Sensors and Actuators B: Chemical, 207, Part A(2015) 518-25.

[10] A.L. Pelé, A. Braud, J.L. Doualan, R. Chahal, V. Nazabal, C. Boussard-Plédel, et al., Wavelength conversion in Er3+ doped chalcogenide fibers for optical gas sensors, Opt Express, 23(2015) 4163-72.

[11] F. Starecki, S. Morais, R. Chahal, C. Boussard-Plédel, B. Bureau, F. Palencia, et al., IR emitting Dy3+ doped chalcogenide fibers for in situ CO2 monitoring in high pressure microsystems, International Journal of Greenhouse Gas Control, 55(2016) 36-41.

[12] A.L. Pelé, A. Braud, J.L. Doualan, F. Starecki, V. Nazabal, R. Chahal, et al., Dy3+ doped GeGaSbS fluorescent fiber at 4.4 μm for optical gas sensing: Comparison of simulation and experiment, Optical Materials, 61(2016) 37-44.

[13] F. Charpentier, F. Starecki, J.L. Doualan, P. Jóvári, P. Camy, J. Troles, et al., Mid-IR luminescence of Dy3+ and Pr3+ doped Ga5Ge20Sb10S(Se)65 bulk glasses and fibers, Materials Letters, 101(2013) 21-4.

[14] W.L. B., C.B.d. Araújo, Y. Ledemi, Y. Messaddeq, Upconversion luminescence in Er3+ doped Ga10Ge25S65 glass and glass-ceramic excited in the near-infrared, Journal of Applied Physics, 113(2013) 083520.

[15] S.D. Wankel, Y.-w. Huang, M. Gupta, R. Provencal, J.B. Leen, A. Fahrland, et al., Characterizing the Distribution of Methane Sources and Cycling in the Deep Sea via in Situ Stable Isotope Analysis, Environmental Science & Technology, 47(2013) 1478-86.